Weakly interacting massive particle diffusion in the solar system including solar depletion and its effect on Earth capture rates

Johan Lundberg*
Division of High Energy Physics, Uppsala University, SE-751 21 Uppsala, Sweden

Joakim Edsjö†
Department of Physics, AlbaNova University Center, Stockholm University, SE-106 91 Stockholm, Sweden
(Received 11 January 2004; published 2 June 2004)

Weakly interacting massive particles (WIMPs) can be captured by the Earth, where they eventually sink to the core, annihilate, and produce, e.g., neutrinos that can be searched for with neutrino telescopes. The Earth is believed to capture WIMPs not dominantly from the Milky Way halo directly, but instead from a distribution of WIMPs that have diffused around in the solar system due to gravitational interactions with the planets in the solar system. Recently, doubts have been raised about the lifetime of these WIMP orbits due to solar capture. We investigate this issue here by detailed numerical simulations. Compared to earlier estimates, we find that the WIMP velocity distribution is significantly suppressed below about 70 km/s, which results in a suppression of the capture rates mainly for heavier WIMPs (above $\sim$100 GeV). At 1 TeV and above the reduction is almost a factor of 10. We apply these results to the case where the WIMP is a supersymmetric neutralino and find that, within the minimal supersymmetric standard model, the annihilation rates and thus the neutrino fluxes are reduced even more than the capture rates. At high masses (above $\sim$1 TeV), the suppression is almost two orders of magnitude. This suppression will make the detection of neutrinos from heavy WIMP annihilations in the Earth much harder compared to earlier estimates.

DOI: 10.1103/PhysRevD.69.123505 PACS number(s): 95.35.+d, 12.60.Jv, 96.35.Cp

I. INTRODUCTION

There is mounting evidence that a major fraction of the matter in the Universe is dark. The Wilkinson Microwave Anisotropy Probe (WMAP) experiment gives as a best fit value that [1] $\Omega_{\rm CDM}h^2=0.113\pm0.009$, where $\Omega_{\rm CDM}$ is the relic density of cold dark matter in units of the critical density and h is the Hubble parameter in units of 100 km s^{-1} Mpc^{-1}. One of the main candidates for the dark matter is a weakly interacting massive particle (WIMP), of which the supersymmetric neutralino is a favorite candidate. There are many ongoing efforts trying to find these dark matter particles, either via direct detection or via indirect detection by detecting their annihilation products.

One of the proposed search strategies is to search for a flux of high-energy neutrinos from the center of the Earth [2]. This idea goes back to Press and Spergel in 1985 [3], who calculated the capture rate of heavy particles by the Sun. For the Earth, the idea is that WIMPs can scatter off a nucleus in the Earth, lose enough energy to be gravitationally trapped, eventually sink to the core due to subsequent scatters, annihilate, and produce neutrinos. For purely kinematical reasons, the capture rate in the Earth depends strongly on the mass and the velocity distribution of the WIMPs. The heavier the WIMP is, the lower the velocity needs to be to facilitate capture. In 1987, Gould [4] refined the calculations of Press and Spergel for the Earth and derived exact formulas for the capture rates. In 1998, Gould [5] pointed out that since the Earth is in the gravitational potential of the Sun, all WIMPs will have gained velocity when they reach the Earth and hence capture of heavy WIMPs would be very small. In that paper, he also analyzed the two possible forms of scattering: *gravitational scattering* and *weak scattering*. Gravitational scattering is elastic and can only change the direction of the orbit, whereas weak scattering is inelastic and can lead to capture of WIMPs. Following the traditions of Öpik [6], equations for the time scales of the various scattering processes were derived.

In 1991, Gould [7] took these ideas further and realized that due to gravitational interactions with the other planets (mainly Jupiter, Venus, and Earth), WIMPs will diffuse in the solar system both between different bound orbits, but also between unbound and bound orbits. Gould showed that the net result of this is that the velocity distribution at the Earth will effectively be the same as if the Earth was in free space (this basically follows from Liouville's theorem). This approximation is widely used today where one further assumes that the halo velocity distribution is Gaussian (i.e., a Maxwell-Boltzmann distribution).

In 1999, the calculations took an unexpected turn, when Gould and Alam [8] interpreted asteroid simulations of Farinella *et al.* [9]. Farinella *et al.* [9] made simulations of about 50 near Earth asteroids (NEAs) that had been ejected from the asteroid belt. They found that about a third of these have lifetimes of less than two million years. After that time they are either thrown into the sun or thrown out of the solar system. If this typical lifetime also applies to WIMPs, this would significantly reduce the number of WIMPs bound in the solar system, as this time scale is shorter than the typical diffusion time scales [7]. This was pointed out by Gould and Alam [8] where they concluded that this in turn would re-

*Electronic address: johan@physto.se
†Electronic address: edsjo@physto.se

duce the expected capture and annihilation rates in the Earth and thus reduce the neutrino fluxes. Gould and Alam investigated two scenarios: an *ultraconservative* scenario where all bound WIMPs are depleted and a *conservative* scenario where all bound WIMPs that do not have Jupiter-crossing orbits are depleted. In the ultraconservative view solar depletion is assumed to be so efficient that no bound WIMPs exist, whereas in the conservative view, Jupiter is assumed to be faster at diffusing WIMPs into the solar system than solar depletion is at throwing them into the Sun. Both of these views significantly reduce the neutrino fluxes from the Earth for heavier WIMPs. In particular they found that in the conservative and ultraconservative view, capture can only occur for WIMPs lighter than about 630 GeV and 325 GeV, respectively. The basic results of Farinella *et al.* were later confirmed by Gladman *et al.* [10] and Migliorini *et al.* [11].

The question to ask, though, is if the results of Farinella *et al.* [9] can really be applied to all Earth-crossing WIMP orbits. The orbits of asteroids ejected from the asteroid belt are, after all, rather special as they typically arise from resonances. It is thus not necessarily so that these results apply to all bound WIMPs. For WIMPs, the truth probably lies somewhere between the conservative view and the usual ''free-space'' approximation in Ref. [7]. The aim of this paper is to investigate the effects of solar capture on the distribution of WIMPs in the solar system and the implication this has on expected neutrino fluxes from the Earth. We will do this by numerical simulations of WIMPs in the solar system and by reanalyzing the process of WIMP diffusion in the solar system. Finally, we will apply our results to the case where the WIMP is the neutralino, which arises naturally in minimal supersymmetric extensions of the standard model (MSSM).

The layout of this paper is as follows. In Sec. II we will go through our assumed halo model and the role of diffusion in more detail. In Sec. III we will go through the formalism for the diffusion caused by one planet and in Sec. IV we add the new ingredient, solar depletion. In Sec. V we present our numerical treatment of the diffusion problem. All of this will be put together with the dominant planets for diffusion in Sec. VI where our main results on the velocity distribution at the Earth are presented. In the remaining sections we will investigate how this affects the capture and annihilation rates in the Earth and will present results on the expected neutrino-induced muon fluxes in MSSM models in Sec. VIII. Finally, we will conclude in Sec. IX.

II. THE GALACTIC HALO MODEL AND CUTOFF MASSES

A. The galactic halo model

In order to make the calculations concrete, we use the Maxwell-Boltzmann model [12], where the local velocity distribution of WIMPs is Gaussian in the inertial frame of the Galaxy. At the location of the Sun the distribution is

$$f_v(v)\mathrm{d}^3v = \frac{e^{-v^2/v_0}}{\pi^{3/2}v_0^3}\mathrm{d}^3v, \tag{1}$$

where $v_0 = \sqrt{\frac{2}{3}}\bar{v}$ with $\bar{v}$ being the three-dimensional velocity dispersion. We will here use the standard value of $\bar{v} = 270$ km/s corresponding to $v_0 = 220$ km/s. The distribution is normalized such that

$$\int f_v(v) 4\pi v^2 \mathrm{d}v = 1. \tag{2}$$

The velocity distribution can be Galileo transformed into the frame of the Sun: $f_s(s)$, where $\mathbf{s} = \mathbf{v} + \mathbf{v}_{\mathrm{Sun}}$, and $v_{\mathrm{Sun}} = 220$ km/s, and averaged over all angles. In this special case of a Gaussian distribution the transformation can be done in closed form [4]. As Gould has pointed out, the angle between the rotation axis of the solar system and that of the galaxy is about 60°, which makes the velocity distribution very close to spherically symmetric, *if one considers averages over a galactic year* ≈ 200 million years [5]. The distribution used is mirror symmetric in the galactic plane, which means that the time of the average need only be 100 million years.

The symbol $F_s(s)$ will be used to denote the phase space number density

$$F_s(s) = \frac{\rho_\chi}{M_\chi} f_s(s), \tag{3}$$

where M_χ is the WIMP mass, and ρ_χ is the WIMP mass per unit volume in the halo. When the particles of this distribution pass through the solar system, the velocities are boosted and focused by the gravitational potential. At the location of the Earth, the solar system escape velocity is $\sqrt{2}v_\oplus \approx 42$ km/s, where we have used the speed of the Earth, $v_\oplus \simeq 29.8$ km/s. Therefore the velocity at the location of the Earth, w, is, according to conservation of energy,

$$w^2 = s^2 + 2v_\oplus^2. \tag{4}$$

When a spherically symmetric distribution such as $F_s(s)$ is focused by a Coulomb potential such as that of the Sun, the following statement holds [5]:

$$\frac{F_w(w)4\pi w^2 dw}{w} = \frac{F_s(s)4\pi s^2 ds}{s}. \tag{5}$$

This can be understood as Liouville's theorem for the spherically averaged phase space density, since

$$\frac{ds}{dw} = \frac{w}{s} \Rightarrow F_w(w) = F_s(s). \tag{6}$$

Since the velocity w of the halo particles is always at least equal to the escape velocity, there will be a hole in velocity space so that

$$F_w(w) = 0 \quad \text{when} \quad w < \sqrt{2}v_\oplus. \tag{7}$$

This is important since capture by the Earth is very sensitive to $F_w(w)$ at low velocities.

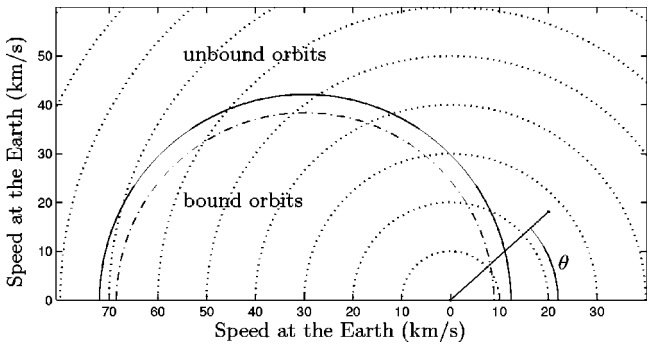

FIG. 1. The ecliptic ($\phi=\pi/2$) slice of the particle velocity space *in the frame of the Earth*. The dotted curves show the velocity relative to the Earth and the indicated angle θ is the angle of the particle with respect to the direction of Earth's motion. The angle ϕ determines in which angle we cut the velocity sphere. $\phi=0$ is the north pole of the solar system and $\phi=\pi/2$ (as shown here) is the slice radially outward from the Earth. The region inside the solid semicircle represents bound orbits. Its radius is the escape velocity from the Solar system at the location of the Earth, but in the frame of the Sun. In the same way, the region outside the dash-dotted line (an almost perfect semicircle) corresponds to particles that may reach Jupiter. By repeated close encounters with the Earth, particles may diffuse along the dotted circles (actually spheres) of constant velocity only, keeping u constant, but allowing changes in θ and ϕ, as explained in the text.

The distribution $F_w(w)$ can now be used to calculate the distribution as seen from the moving Earth where the particle velocity is $\mathbf{u}=\mathbf{w}+\mathbf{v}_\oplus$:

$$F_u(\mathbf{u})=F_w(\mathbf{w})=F_w(\mathbf{u}-\mathbf{v}_\oplus). \tag{8}$$

This means that the *hole* is shifted, so that it is centered around $-\mathbf{v}_\oplus$. This is visualized by Fig. 1, which displays a two dimensional slice of the three dimensional velocity space.

B. Cutoff masses when low velocity WIMPs are missing

In the absence of WIMPs gravitationally bound to the solar system, the capture by the Earth is totally suppressed for WIMP masses larger than a critical value. A particle approaching the Earth with velocity u at infinity will need to be scattered off an atom to a velocity less than the escape velocity, $v_{\rm esc}$, to be captured. Assuming iron to be the heaviest relevant element of the Earth, this means that the particle must have a velocity less than

$$u_{\rm cut}=2\frac{\sqrt{M_\chi M_{\rm Fe}}}{M_\chi-M_{\rm Fe}}v_{\rm esc} \tag{9}$$

to be capturable. Solving for the WIMP mass M_χ gives

$$M_{\chi,{\rm cut}}=M_{\rm Fe}\frac{u^2+2v_{\rm esc}(v_{\rm esc}+\sqrt{u^2+v_{\rm esc}^2})}{u^2}, \tag{10}$$

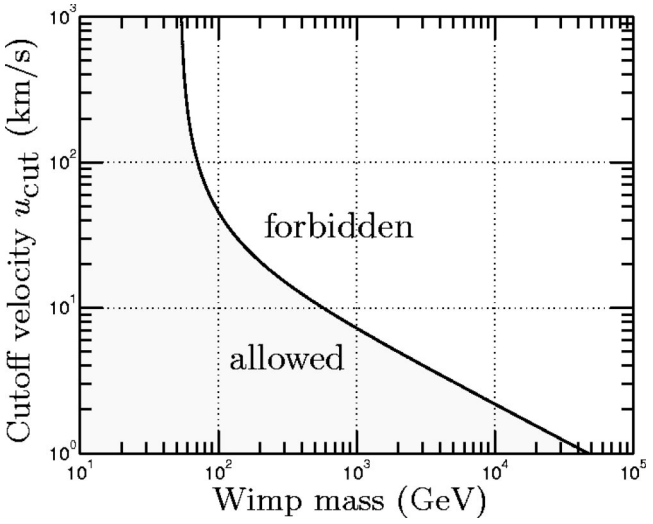

FIG. 2. Cutoff velocity $v_{\rm cut}$ against WIMP mass M. Only combinations of M and $v_{\rm cut}$ to the left of the line are kinematically allowed (in the sense that they can lead to capture by the Earth).

where u is the speed (at infinity) of the approaching particle in the frame of the Earth and $M_{\chi,{\rm cut}}$ is the highest allowed mass of the particle if it is to be captured by the Earth. The escape velocity varies from 11.2 km/s at the surface to 15.0 km/s at the center of the Earth (see Sec. VII A for more information about the Earth model we use), and capture is thus easiest at the center where the escape velocity is higher. Using $v_{\rm esc}=15.0$ km/s, we plot in Fig. 2 the relation between $u_{\rm cut}$ and the cutoff mass, $M_{\chi,{\rm cut}}$.

With Eq. (10), we can now relate to the cutoff masses in the conservative and ultraconservative views by Gould and Alam [8]. In the ultraconservative view, we assume that only unbound halo particles are captured. Halo particles cannot be slower than $u_{\rm cut}=(\sqrt{2}-1)v_\oplus\simeq 12.3$ km/s at, and in the frame of, the Earth (this is also seen in Fig. 1). This gives a cutoff mass of about 410 GeV over which capture by the Earth is impossible. In the conservative view, we assume that Jupiter-crossing orbits are filled. This means that all orbits outside the dot-dashed curve and the dashed curve in Fig. 1 are filled. The lowest velocity WIMP at the Earth that is on a Jupiter-crossing orbit is in the lower right-hand end of the dot-dashed curve and it has a velocity of $u_{\rm cut}=v_\oplus[\sqrt{2/(1-r_\oplus/r_{2\perp})}-1]\simeq 8.8$ km/s (and is moving in the same direction as the Earth). $r_{2\perp}\simeq 5.2r_\oplus$ is the radius of the Jupiter orbit. This value of $u_{\rm cut}$ gives a cutoff mass of about 712 GeV. These cutoff masses agree roughly with the ones by Gould and Alam [8] (325 GeV and 630 GeV, respectively). The differences are due to different escape velocities used and an approximation in their treatment of Jupiter-crossing orbits [31].

If, on the other hand, the solar system is full of gravitationally bound dark matter, the velocities can be much lower. As the lowest allowed velocity of the WIMPs $u_{\rm cut}$ tends to zero, the mass limit $M_{\chi,{\rm cut}}$ goes to infinity.

III. GRAVITATIONAL DIFFUSION IN THE ONE-PLANET CASE

A particle in close encounter with a planet, for instance the Earth, may get gravitationally scattered into a new direction and a new velocity *as seen from the frame of the Sun*. However, by conservation of energy, the speed *u with respect to the frame of the planet* is unchanged. This means that a particle at a particular place in velocity space may, by repeated close encounters with the Earth, diffuse to any location on the sphere of constant velocity (with respect to the Earth), and nowhere else.

The location of a particle at such a sphere can be specified by the angles at which it passes the Earth. The angle θ is measured between the forward direction of the Earth and the velocity vector of the particle, and ϕ is the angle of rotation around the forward direction of the Earth, with $\phi=0$ at the north pole of the solar system. Figure 1 illustrates how spheres (and circles) of constant u cross the limit of where particles have bound and unbound orbits. This corresponds to the possibility of gravitational capture and ejection from the solar system.

A single planet can diffuse particles along spheres of constant velocity only. In this section, we will investigate the gravitational diffusion caused by one planet, and will take the Earth as an example. We will here develop tools for detailed investigation of the bound orbit phase space density, taking the effects of solar depletion into account. We assume that when a particle is in Earth-crossing orbit (perihelion less than the Earth orbit radius $R_\oplus$ and aphelion greater than $R_\oplus$), long range interactions with other planets are less important, and can be ignored. This is not a problem, as we in Sec. VI add the effects of other planets (apart from possible resonances). We will in this section closely follow Gould [7], with some small modifications.

A. The probability of planet collisions

We are interested in calculating the rate at which WIMPs with Earth-crossing orbits come into close encounter with the Earth. This will be used to estimate how the Earth affects the WIMP distribution. A close encounter is an event were the particle's impact parameter is smaller than or equal to some value $b_{max}(u)$.

Let's imagine the Earth as being spread out on a flat ring of inner radius R, outer radius $R+l$, and thickness h, as in Fig. 3. Now consider a particle with perihelion less than the planet orbit radius R and aphelion greater than R. Such particles will be said to have Earth-crossing orbits. This is motivated by the fact that due to the precession of perihelion, all such orbit ellipses will eventually intersect the Earth ring. The small angle the perihelion sweeps out, as the orbit ellipse enters and leaves the ring, is given by

$$\Delta\xi \approx \tan\Delta\xi = \frac{l}{R}|\tan\Theta_1|, \tag{11}$$

where Θ_1 is the intersection angle between the WIMP ellipse and the plane perpendicular to the location vector of the Earth **R**. Since this happens four times during each perihelion revolution, the mean probability for such a WIMP to intersect the ring of the Earth during each WIMP year T_χ is

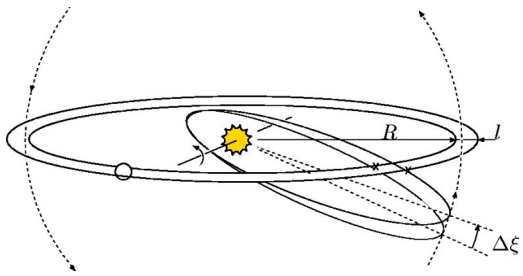

FIG. 3. The angle of perihelion precession $\Delta\xi$, as the orbit enters and leaves the disk of the Earth. In this example, the plane of the orbit is nearly perpendicular to the ecliptic plane.

$$\langle p_{T_\chi}\rangle = \frac{4\Delta\xi}{2\pi}. \tag{12}$$

The probability for the WIMP to come into close encounter with the Earth is therefore p_{T_χ} times the cross section σ of such an event, divided by the area over which the Earth is distributed. However, the length of the path that is inside the Earth ring during each encounter is $\propto|\cos\Theta_2|^{-1}$, where Θ_2 is the angle between the axis of the ecliptic and **u** is the velocity of the WIMP as seen from Earth [5]. The probability for a reaction with cross section σ can now be calculated,

$$\frac{p(\sigma)}{T_\oplus} = \frac{1}{|\cos\Theta_2|}\frac{\sigma}{2\pi Rl}\frac{4l}{2\pi R}|\tan\Theta_1|\frac{1}{T_\chi}, \tag{13}$$

where we have divided by $T_\oplus$ to get the probability per unit time. The WIMP year can be written in terms of $\mathbf{u}(\theta,\phi,u)$ [5], the velocity of the particle in the frame of the Earth,

$$T_\chi = \left(1-2\frac{u}{v_\oplus}\cos\theta-\frac{u^2}{v_\oplus^2}\right)^{-3/2}T_\oplus, \tag{14}$$

and $\Theta_1(\mathbf{u})$ and $\Theta_2(\mathbf{u})$ can be expressed in u, θ, and ϕ:

$$\cos\Theta_1 = \hat{\mathbf{R}}\cdot\hat{\mathbf{v}}_\chi = \frac{\mathbf{R}\cdot(\mathbf{u}+\mathbf{v}_\oplus)}{R|\mathbf{u}+\mathbf{v}_\oplus|} = \frac{u\sin\theta\sin\phi}{(u^2+v_\oplus^2+2uv_\oplus\cos\theta)^{1/2}}, \tag{15}$$

$$\cos\Theta_2 = \sin\theta\cos\phi = \frac{\mathbf{u}\cdot(\mathbf{v}_\oplus\times\mathbf{R})}{uv_\oplus R}, \tag{16}$$

$$\cot\Theta_1 = \frac{u}{v_\oplus}\frac{\sin\theta\sin\phi}{[1+2(u/v_\oplus)\cos\theta+(u^2/v_\oplus^2)(1-\sin^2\theta\sin^2\phi)]^{1/2}}. \tag{17}$$

By substituting and rearranging we conclude that the yearly reaction probability for an event with cross section σ is given by

$$\frac{p(\sigma,\mathbf{u})}{T_\oplus} = \frac{3}{2}\frac{\sigma}{\pi R^2}\frac{v_\oplus}{u}\gamma(\mathbf{u})^{-1}, \tag{18}$$

where

$$\gamma(\mathbf{u}) = \frac{3}{2}\frac{\pi\sin^2\theta|\sin\phi\cos\phi|(1-2u/v_\oplus\cos\theta-u^2/v_\oplus^2)^{-3/2}}{[1+2(u/v_\oplus)\cos\theta+(u^2/v_\oplus^2)(1-\sin^2\theta\sin^2\phi)]^{1/2}}. \tag{19}$$

Equation (19) was first derived by Gould [5] in a very similar way. Among other things, he used it to calculate the ''typical time scales'' at which particles diffuse between different velocity space regions in the absence of solar depletion. It is also used for calculating the probability of weak scattering of WIMPs at the Earth.

The equations above are derived under some (geometrical) approximations with the aim of getting the correct scattering probabilities on average. There are, however, a few pathological cases where the geometrical model used above breaks down. This happens when $\phi=0$, $\phi=\pi/2$, $\theta=0$, and $\theta=\pi$, in which case the probabilities above are unphysical. Since this only happens for these few special cases we will artificially solve this by adding a small angle (of about 1°) to θ and ϕ when close to these regions. Note that in principal, the problems could be resolved, by making $\Delta\xi$ a function of the full set of orbit parameters, but this is unnecessarily complicated for our purposes. For the interested reader, we refer to a detailed investigation of the mathematical properties of γ as presented in Refs. [5] and [7]. To test our solution of adding a small angle in these pathological cases, we have investigated the effect of further increasing the small angle added and conclude that the actual value chosen is not important for the final results. This is reasonable, since orbits in the vicinity of these critical regions are quickly deflected into other orbits anyway.

B. Gravitational scattering on a planet

Now that we have learned how to calculate the probability for particles to come into close encounter with a given planet, it is time to apply this to gravitational diffusion. For the Earth, we were mainly interested in those particles crossing the sphere of 1 A.U. during each revolution, since they have a chance of hitting the Earth (and possibly be weakly captured to it) within each perihelion precession revolution.

The gravitational scattering probability is dependent on the angular distance between the velocities before and after scattering, $\mathbf{u}$ and $\mathbf{u}'$, such that small deflections are more common. The angle can be related to the impact parameter b,

$$\delta(b) = \pi - 2\arctan\frac{bu^2}{MG}, \tag{20}$$

as well as

$$\delta(\hat{\mathbf{u}}',\hat{\mathbf{u}}) = \arccos(\hat{\mathbf{u}}'\cdot\hat{\mathbf{u}}), \tag{21}$$

where the caret denotes unit vectors. The scattering angle above is the one given by Rutherford scattering (see, e.g., Ref. [13]). Gould used an approximate formula when deriving the typical time scales [4]: $\delta(b)=R_\oplus v_{\rm esc}^2/(bu^2)$. The two differ at very small impact parameters, and we use the full expression in our calculations.

As mentioned before, scattering can only change the direction and not the velocity, and we are therefore dealing with random walk on spheres of constant u. The direction η of the scattering is evenly distributed, as seen in Fig. 4, where the scattering setup is shown. The arc length is fixed by $\delta(b)$, but the scattering *direction* is evenly distributed.

The cross section for scattering between δ and $\delta+d\delta$ is $d\sigma=2\pi b db$, so the yearly probability for scattering in this range is [using Eq. (18)]

$$\frac{dp(\mathbf{u},b)}{dbT_\oplus} = \frac{3}{2}\frac{2\pi b}{\pi R^2}\frac{v_\oplus}{u}\gamma(\mathbf{u})^{-1}. \tag{22}$$

This can be rewritten in terms of the scattering angle $\delta(\hat{\mathbf{u}}',\hat{\mathbf{u}})$,

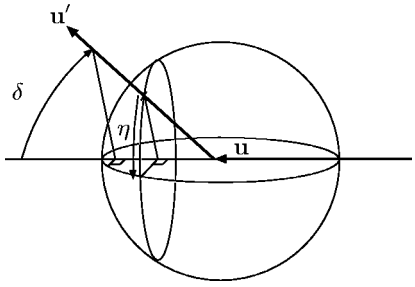

FIG. 4. Scattering off the Earth in velocity space. A fixed impact parameter fixes δ, but η is evenly distributed.

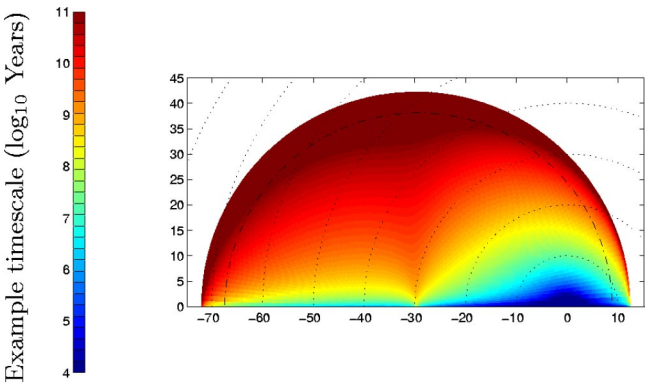

FIG. 5. (Color online). An example of the time scales of particle scattering. The color bar indicates the time for which there is a 10% probability of scattering an angle $\delta=\pi/2\pm\pi/64$, depending on the present location of the particle. In general, time scales are shorter at lower velocities. By repeated close encounters with the Earth, particles may diffuse along the dotted circles (actually spheres) of constant velocity only, keeping u constant, but allowing for changes in θ and ϕ. The figure shows the $\phi=75°$ slice of the particle velocity space only.

$$\frac{dp(\mathbf{u},b(\delta))}{d\delta T_\oplus}=-\frac{3}{2}\frac{2\pi}{\pi R^2}\frac{v_\oplus}{u}\gamma(\mathbf{u})^{-1}\frac{(M_\oplus G)^2}{u^4}\times\frac{\cos[\delta(\hat{\mathbf{u}}',\hat{\mathbf{u}})/2]}{2\sin^3[\delta(\hat{\mathbf{u}}',\hat{\mathbf{u}})/2]} \tag{23}$$

since

$$b=\frac{M_\oplus G}{u^2}\cot\frac{\delta}{2},\quad \frac{db}{d\delta}=-\frac{M_\oplus G}{u^2}\frac{1}{2\sin^2(\delta/2)}. \tag{24}$$

The right-hand side of Eq. (23) may look like a negative probability density, but this is artificial since integration should be done for decreasing δ's. We integrate Eq. (23) analytically and use that expression whenever numerical values of the scattering probability to $\delta+\Delta\delta$ are needed.

To get a feeling for the significance of the diffusion, we solve Eq. (23) to obtain the typical time scales for scattering a given angle to occur. As an example, we look at the time scales for which the probability of scattering with $\delta=\pi/2\pm\pi/64$ is 10%. This is illustrated in Fig. 5.

C. The bound orbit density and orbit capture from the halo

Let us now define *the bound orbit density* $n(\mathbf{u})$ to be the number of bound particle *orbits* per infinitesimal velocity and solid angle on the velocity sphere. The orbit density is thus free from information about the particle location along its elliptical orbit. The total number of bound particle orbits in a thin shell of radius u is

$$dN=duu^2\int\int_{\Omega=\text{bound orbits}}d\Omega n(\mathbf{u}). \tag{25}$$

We will now divide each velocity sphere into cells (that can at this point be viewed as infinitesimally small). The number of particles scattered between two locations on a sphere of constant velocity in a given time must be an integral over the source cell i and the destination cell j,

$$\frac{dN_{ji}}{dt}=\int\int_{\alpha\in\Omega_i}\int\int_{\beta\in\Omega_j}\frac{dP(\beta,\alpha)}{dt}n(\alpha).$$

In our case, the destination space is conveniently spanned by the scattering angles δ and η. The density of bound orbits scattered from cell i to cell j evolves with time as

$$\frac{dn_{ji}}{dt}=\int\int_{\Omega_i}d\Omega\int\int_{K_j}d\delta\frac{d\eta}{2\pi}\frac{dp(\mathbf{u},\delta)}{d\delta T_\oplus}n(\mathbf{u}), \tag{26}$$

where K_j is defined to be the region in δ-η space corresponding to scattering from the i to the j cell. The scattering probability to the $[\delta,\delta+\Delta\delta]$ band is evenly distributed over all cells in that region. Numerically this is implemented as loop over δ as measured from the center of the source cell. The probability is then distributed over all discrete cells whose centers are inside the current band.

Note that we here consider the movement of particle orbits, as opposed to the particles themselves. When we are interested in the actual particle densities, we have to convert from orbit to particle densities.

The equations derived above apply only to particles which are already gravitationally bound to the solar system. We now turn to the calculation of the *bound orbit density capture rate*; $\Delta n_{jf}/T_\oplus$ from the distribution of free particles. We will use the local phase space density $F_f(\mathbf{u})[\text{particles}/(\text{m}^3\,\text{m/s})]$.

Consider the distribution of particles $F_f(\mathbf{u})$ passing the Earth with impact parameter b. The number of particles scattered an angle $\delta(b\pm db/2)$ in a given period of time T is

$$\underbrace{Tu2\pi bdb}_{dV}F_f(\mathbf{u}). \tag{27}$$

According to Eq. (20) they are scattered at an angle $\delta(b)$. Using the relations (24) we conclude that the *bound orbit density* at the cell j will evolve with time as

$$\frac{dn_{jf}}{dt}=\int\int_{\Omega_{\text{free}}}d\Omega\int\int_{K_j}d\delta\frac{d\eta}{2\pi}\times\left(-2\pi u\frac{(M_\oplus G)^2}{u^4}\frac{\cos(\delta/2)}{2\sin^3(\delta/2)}F_f(\mathbf{u})\right), \tag{28}$$

caused by gravitational scattering from the halo. We now have equations for gravitational diffusion as well as capture to the solar system.

D. Relating the phase space density $F(\mathbf{u})$ and the bound orbit density $n(\mathbf{u})$

The ideas of the preceding section can be used to write down an expression for the phase space density, which we

need for the weak capture calculations. The relation between the phase space density $F(\mathbf{u})$ and the *bound orbit density*; $n(\mathbf{u})$ is derived as follows.

For a given orbit in the population of bound orbits, we use Eq. (18) to calculate the number of orbits that will pass trough an area σ each year. We now consider a volume dV in space with base area σ and height h such that h is parallel to $\mathbf{u}$. A particle passing through the area will spend a time h/u in the volume. This means that the fraction of the WIMP year spent in the volume in case of an encounter is

$$\frac{h}{uT_\chi}.$$

The fraction of orbits passing through σ each WIMP year is

$$\frac{p(\sigma,\mathbf{u})}{T_\oplus}T_\chi.$$

Therefore, since $F(\mathbf{u})$ is the number of particles per du^3dV, the relation between $F(\mathbf{u})$ and $n(\mathbf{u})$ is

$$F(\mathbf{u})\mathrm{d}V = n(\mathbf{u})\frac{h}{uT_\chi}\frac{p(\sigma,\mathbf{u})}{T_\oplus}T_\chi \tag{29}$$

or

$$F(\mathbf{u})\mathrm{d}V = n(\mathbf{u})h\frac{p(\sigma,\mathbf{u})}{uT_\oplus} = n(\mathbf{u})\frac{3}{2}\frac{\mathrm{d}V}{\pi R^2}\frac{v_\oplus}{u^2}\gamma(\mathbf{u})^{-1}. \tag{30}$$

IV. SOLAR DEPLETION OF BOUND ORBITS

In the preceding section, we investigated the evolution of the bound orbit densities due to scatterings from other bound orbits and from free orbits. One main piece remains to be studied, and that is the effects of solar depletion, i.e., how much of the bound WIMPs are actually captured by the Sun, thus reducing their density in the solar system.

We have done this by numerically calculating the actual motion for different WIMP orbits in the solar system over 49 million years. As a measure of the quality of the numerical methods, we have also calculated the fates of the 47 asteroids studied by Farinella *et al.* [9], as presented in the Appendix.

A. The numerical methods and conditions

We have numerically integrated the orbits of about 2000 particles in typical Earth-crossing orbits in order to estimate the solar depletion. The particles were spread out on the bound velocity space with random initial positions on the Earth's orbit. We have mainly used the MERCURY package [14] by Chambers for the integration. It has the most important numerical algorithms, such as Everhart's 15th order Radao [15] algorithm with Gauss-Radao spacings, and the equally well-known Bulirsch-Stoer [16] algorithm. Both are variable step size algorithms dedicated to many body problems, and are commonly used in asteroid research for problems similar to ours. The package also includes a set of symplectic algorithms, which have been used for some tests. By looking at some test orbits, we found that the symplectic algorithms (at least as implemented in the MERCURY package) were slower and less accurate for our setup. The tested symplectic algorithms were ''MVS: mixed-variable symplectic'' [17] as well as ''hybrid symplectic/Bulirsch-Stoer'' [14].

The calculations included the test particles, the Sun, the Earth, Jupiter, and Venus. Other planets were not included as they are believed to be subdominant. The Bulirsch-Stoer algorithm was used to calculate the orbits of all test particles, as well as the planets, during a time of 49 million years. This took about 35 000 CPU hours, on a variety of Linux and Alpha machines. A wide range of different accuracy parameters was used, from 10^{-14} to 10^{-8}, to evaluate the role this plays. The numerical representation of the real numbers limits the benefit of going past about 10^{-12}. The final choice of 10^{-10} is a balance between time and accuracy. A recent publication [18] in the subject of numerical simulations of a special set of Jupiter-crossing asteroids came to a similar conclusion. When using the Bulirsch-Stoer algorithm for their calculations, Ipatov and Mather found accuracy parameters in the range 10^{-9}–10^{-8} to give statistically similar results as 10^{-12}. In the comparisons carried out, this gave results very similar to those with higher accuracy parameters. The comparison with the Radao algorithm gave qualitatively similar, however, not identical results with a similar calculation speed. In some occasions, however, the Radao algorithm gave a higher solar depletion for particles with very high velocity (relative to the Earth), $u \gtrsim 50$ km/s. This is not of much concern for our purposes though as we are mainly interested in much lower velocities for Earth capture to be efficient.

For ordinary asteroid calculations, a point mass approximation combined with collision detection is sufficient. Our case is a little more delicate since WIMPs may pass through the planets. To handle this, the gravitational routines were modified to use the real gravitational potentials inside the planets.

For Jupiter and Earth, we used ''true'' mass distributions [19,20]. For Venus we rescaled the mass distribution of the Earth and removed the liquid iron core [32]. Other planets included in tests where assumed to be homogeneous. The improvement allows the particles to pass through the planets without being infinitely scattered by a point mass, making the calculations more realistic and numerically stable. For completeness, it would be interesting to add more planets to the simulations, but it is unfeasible to do as it slows down the calculations too much. We also believe that we have included the most important planets in our simulations.

B. The results of the numerical simulations

The solar depletion was mainly calculated for particles in eight planes of $\mathbf{u}$ space, with the ϕ values 0, 15, 30, 45, 60, 75, 90, and -30 degrees (the $\phi = -30°$ plane was used to investigate the expected radial mirror symmetry of the results). Our solar depletion results are not as bad as Gould feared [8]; Most of the particles survived two million years. Nevertheless, solar capture is too large to be ignored. Figure 6 show the $\phi = 75°$ plane, and the times after which the

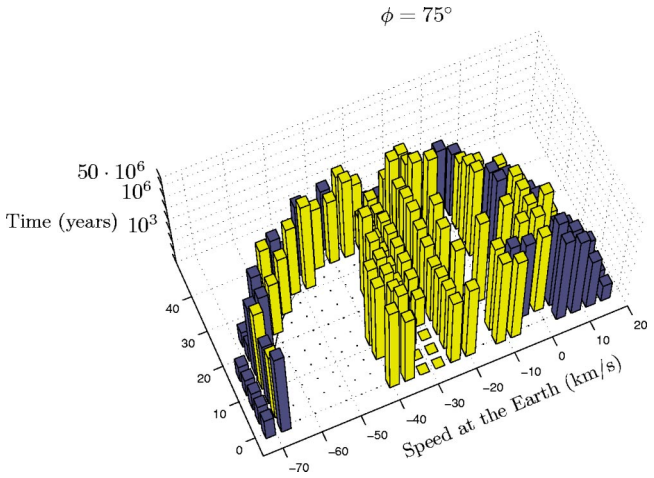

FIG. 6. (Color online). The time for ejection (blue/dark gray) and capture in the Sun (yellow/light gray) of a set of test particles. Each bin represents only one particle, so the statistical error is high. However, this figure is typical for all angles, except that the plateau of fast solar depletion at large ''backward'' velocities are raised when ϕ approaches 90°. Some particles survived in the solar system for the whole of the simulation. Those particles are marked with black dots. It is easy to see that there is a small region at -30 km/s where the solar depletion occurs directly. This is not surprising, since this region corresponds to particles with very low velocity *in the frame of the Sun*. The plateau of direct solar capture extends further in the special case of $\phi = 90°$ (not shown) which allows extremely elliptic, or radial orbits. (The plane of start positions is then parallel to the ecliptic plane.)

particles hit the Sun. We note that ejection is much more common at Jupiter-crossing orbits. This is in compliance with the fact that, according to the scattering model used here, the probability of scattering for such orbits is high. The fact that there is a large region at -50 km/s where there are no ejections or Sun captures, is in agreement with the qualitative results by Gould, presented in his 1991 paper [7] (see his Fig. 3, where he assumes that the filling times are about the same as the time of ejection). Apart from the calculations shown here, some extra calculations were carried out for relative velocities lower than 15 km/s. The results of those calculations were incorporated and used in the same way as the others.

Another important, however, simple result is that there seems to exist a mirror symmetry in the in-out directions. This is expected, since particles may hit the Earth both on its way out and on the way back on its perihelion revolution. Considering Fig. 3, it is evident that this is equivalent to a symmetry in the sign of ϕ claimed by Gould, that the ϕ and $-\phi$ cases are identical.

The particle orbits were evenly distributed in velocity space, but we solve the diffusion equations on spheres of constant u; hence we interpolate our results. From our numerical simulations we then extract the depletion frequency, i.e., the expected depletion probability per given time. Since the form of the actual distribution, of which the results of the numerical calculations are samples, is unknown, the most reasonable way to estimate the depletion probability per unit time is

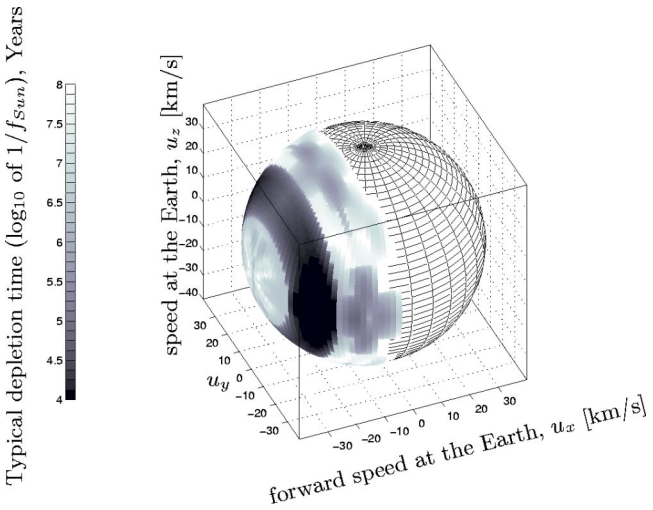

FIG. 7. (Color online). The solar depletion at the $u = 40$ km/s sphere. The color bar indicates the logarithm of the typical depletion time $1/f_{Sun}$. The region to the right are the free orbits, for which the solar depletion is irrelevant. At a ''backward'' velocity of 30 km/s, the Sun depletion is greater, in agreement with the previous figures of this section. In understanding this figure, it may help to take a look at the $u = 40$ km/s line of Fig. 1, which corresponds to the central horizontal ($\phi = 90°$) plane of this figure.

$$f_{Sun} = \frac{1}{T_{Sun}}. \tag{31}$$

Figure 7 shows the logarithm of $1/f$, interpolated onto a sphere of constant u, namely $u = 40$ km/s.

V. THE EVOLUTION EQUATIONS FOR ONE PLANET

In the previous sections we have presented the analytic expressions for the scattering of bound orbits to other bound orbits, Eq. (26), as well as capture from free to bound orbits, Eq. (28). We have also, by numerical simulations, estimated the rate at which orbits are sent into the Sun and thus captured. We are primarily interested in how the bound orbit density evolves with time, and will here write down the dynamic equations in a form suitable for numerical work.

A. The dynamic equations of the bound orbit density

The bound orbit density develops in time in the following way:

$$du\, u^2 \frac{dn_j}{dt} = du\, u^2 \left[\sum_{i \in \text{bound}} \left(\frac{dn_{ji}}{dt} - \frac{dn_{ij}}{dt} \right) + \sum_{f \in \text{unbound}} \left(\frac{dn_{jf}}{dt} - \frac{dn_{fj}}{dt} \right) - \frac{dn_{sj}}{dt} \right], \tag{32}$$

where n_j is the number of orbits in the small cell [33] j of the sphere. The sum over i is the flow from and to the other bound cells. The n_{jf} and n_{sj} terms are representing capture from unbound orbits and capture of bound orbits by the Sun, while the n_{fj} term represents the ejection of bound particles.

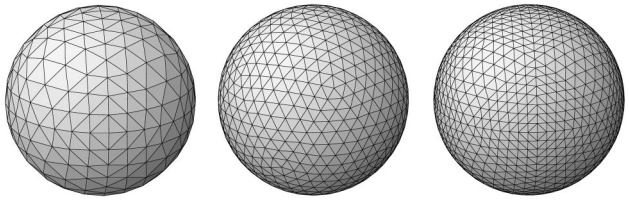

FIG. 8. The discretization of space was made using triangles. The number of cells on the displayed triangles are 512, 1280, and 2048, of which the last one was used in our final calculations.

We will now reformulate Eq. (32) in matrix form suitable for numerical calculations. Let us first define our state vectors,

$$X=\begin{pmatrix} N_s \\ n_i \\ F_f \end{pmatrix}, \tag{33}$$

where N_s is the number of particles captured by the Sun, n_i is the bound orbit density, and F_f is the velocity number density of free (unbound) orbits. We can then write the evolution of the state vector during a time step Δt as

$$X(t_0+\Delta t)=\mathbf{T}(\Delta t)X(t_0),$$

with

$$\mathbf{T}(\Delta t)=\begin{pmatrix} 1 & \mathbf{P}^{\mathrm{sc}} & \mathbf{0} \\ \mathbf{0} & \mathbb{1}+\mathbf{P}^{\mathrm{bb}}(\mathbb{1}-\mathbf{P}^{\mathrm{sc}})-\mathbf{P}^{\mathrm{sc}} & \mathbf{P}^{\mathrm{bf}} \\ \mathbf{0} & \mathbf{0} & \mathbb{1} \end{pmatrix}, \tag{34}$$

where the matrices $\mathbf{P}$ can be regarded as transition probabilities (for the given time interval Δt). $\mathbf{P}^{\mathrm{sc}}$ contains the probability of solar capture, extracted from the numerical simulations in Sec. IV, whereas $\mathbf{P}^{\mathrm{bb}}$ and $\mathbf{P}^{\mathrm{bf}}$ describes the development of bound orbits and the capture of free orbits, respectively. The relevant quantities for the latter are read off from Eqs. (26) and (28). The last row is a little bit special. One may propose that bound WIMPs scattered to unbound orbits should give a contribution in the second column. However, such particles will not meet the Earth again, so the lowest part of the matrix should only do the job of keeping the unbound phase space density constant.

B. The bound orbit density at arbitrary times

Equation (34) describes the evolution of the state vector X during a time step Δt. We can write the time development operator that takes us to any time t as

$$\mathbf{U}(t)\equiv[\mathbf{T}(\Delta t)]^{t/\Delta t}, \quad X(t_0+t)=\mathbf{U}(t)X(t_0). \tag{35}$$

The exponentiation of $\mathbf{T}$ can be done either by diagonalizing $\mathbf{T}$, or (for applicable times t) by repeatingly quadrating $\mathbf{T}$. We have calculated and diagonalized $\mathbf{T}$'s with a variety of different cell configurations. A simple polar grid is a good first choice, but it has a large spread in shape and area of the cells, which means that valuable memory and calculation time is wasted. Therefore, we have used cells with the shape of spherical triangles, built from icosahedrons or octahedrons, as shown in Fig. 8. The cells of the body were successively divided in four nearly identical spherical triangles, until the right number of cells were reached. The velocity space of each planet was built up of about 65 spheres, usually with 2048 cells each, which means a total of about 130 000 discrete cells for each planet.

If the octahedron is used as a starting object, it is possible to rotate the sphere to obtain mirror symmetry in the in-out (radial in the solar system) and up-down directions. Since the problems to solve possess the same symmetries, this reduces the size of the state vectors by a factor of four, and the time evolution operators by a factor of 16.

Great efforts have been put in verifying the consistency of the time evolution operator. As a simple example, the probability for a particle to end up *anywhere* is unity. Making use of the mirror symmetry of the equations, it has been possible to calculate and diagonalize P's with up to some 10^8 elements. We have also checked the robustness of our results as the number of cells varies. If one uses too few cells, one would expect that the effect of diffusion is underestimated as small-angle deflections (smaller than the cell size) are then artificially suppressed. At velocities above 8 km/s, our results do not change significantly when going from 1024 to 2048 cells. Below 8 km/s, however, the resulting WIMP density is somewhat larger in our simulation with 2048 cells than in our simulation with 1024 cells. This would indicate that the density at these low velocities could go up somewhat if we used even more cells. However, it is not possible to increase the number of cells further, as it is only feasible to perform these simulations when the full velocity space can be maintained in the computer memory simultaneously. It is also not reasonable to perform this part of the calculation more accurately than other parts, like the solar capture discussed in the preceding section.

We have now set up a framework for diffusion from one planet. We have done this following the scheme set up by Gould [7], with some small modifications and improvements. Our main goal has been to make it possible to include the effects of solar depletion, and hence we have formulated the diffusion problem in a form suitable for numerical work, where the inclusion of solar capture is easily done.

VI. THE VELOCITY DISTRIBUTION AT THE EARTH: COMBINING THE EFFECTS OF JUPITER, VENUS, AND THE EARTH

We have so far considered the diffusion caused by one planet at a time and the effect of solar capture. We are now ready to include more than one planet in our treatment. In Sec. III, where we investigated the diffusion effects caused by one planet, we saw that one planet can only change the direction and not the velocity of a WIMP. However, WIMPs that have different directions but the same velocity at one planet will not only have different directions, but also different velocities at another planet. Hence, the main effect of

including more planets in the diffusion is to diffuse particles also to different velocities. We thus have a mechanism to populate a larger part of the phase space at Earth, and this process is hence very important, especially for heavier WIMPs. We will here include the diffusion effects of Venus, the Earth, and Jupiter as these are the planets dominating the diffusion mechanism [7].

A. Transformation of coordinates and bound orbit density when changing planets

The velocity and angles in a planet-based coordinate system at a planet with orbit radius a and velocity v can be converted to the coordinates of another planet via the energy, angular momentum, and inclination. This is not enough for the specification of the exact location of the particles, but we are only interested in the shape and orientation of the *orbits*,

$$E=\frac{1}{2}\left(u^2+2uv\cos\theta+v^2-2\frac{M_\odot G}{a}\right), \tag{36}$$

$$L=a(v+u\cos\theta), \tag{37}$$

$$\tan i=\frac{u\sin\theta\cos\phi}{v+u\cos\theta}. \tag{38}$$

The inverse transformation is

$$u^2=2\left(E-L\frac{v}{a}+\frac{1}{2}v^2+\frac{M_\odot G}{a}\right), \tag{39}$$

$$\cos\theta=\frac{1}{u}\left(\frac{L}{a}-v\right), \tag{40}$$

$$\cos\phi=\frac{L\tan i}{au\sqrt{1-\cos^2\theta}}. \tag{41}$$

As an example, we will transform the various densities, as seen in the frame of the Earth to the corresponding quantities at Venus.

The change of frame consists of two Galileo transformations, as well as the journey of the particles in the potential force of the Sun. Since the first is just a change of origin in the six-dimensional phase space, the change of frame obeys Liouville's theorem,

$$F_\varphi(\mathbf{u}_\varphi)=F_\oplus(\mathbf{u}_\oplus). \tag{42}$$

Using Eq. (30), the orbit densities at the two locations can now be related as

$$n_\varphi(\mathbf{u}_\varphi)=n_\oplus(\mathbf{u}_\oplus(\mathbf{u}_\varphi))J_{\oplus\varphi}(\mathbf{u}_\varphi), \tag{43}$$

where

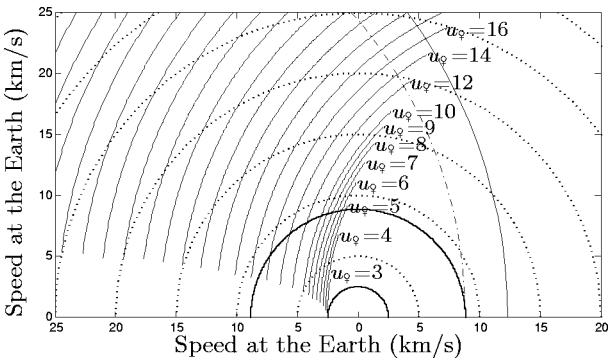

FIG. 9. The $\phi=75°$ slice of the particle velocity space at the frame of the Earth. The solid arcs represent particles in Venus-crossing orbits, and their speed *at the location and in the frame of Venus*. Since the arcs are part of spheres of constant velocity at Venus, they show the possible directions of diffusion caused by Venus. The region outside the solid $u\approx 9$ km/s line is populated by the combined effect of Jupiter and the Earth. The diffusion effect of Venus is needed for particles to reach the region between the 9 km/s and 2.5 km/s lines.

$$J_{\oplus\varphi}(\mathbf{u}_\varphi)=\frac{v_\oplus}{v_\varphi}\left(\frac{R_\varphi u_\varphi}{R_\oplus u_\oplus(\mathbf{u}_\varphi)}\right)^2\frac{\gamma_\varphi(u_\varphi)}{\gamma_\oplus(u_\oplus(\mathbf{u}_\varphi))} \tag{44}$$

is the Jacobian.

Using these transformations, it is possible to investigate how a sphere of constant velocity at a specific planet will look when the particles pass the Earth. Figure 9 is an example of this.

The arcs of constant velocity *in the frame of Venus* are shown to indicate the directions of diffusion caused by that planet. Since the lines of constant velocity at Venus cross the $u_\oplus=12.3$ km/s line, Venus may diffuse particles into the important $u_\oplus<12.3$ km/s region.

B. Solving the many body diffusion problem

Consider a point in velocity space, in the frame of the Earth, *and in the Jupiter-crossing orbit*. At this point, the bound orbit density $n(\mathbf{u})$ takes on a value n_A at a given time t_0. Call this density, transformed into a specific point in the reference frame of Jupiter n_B. Now, after a short period of time, from now on called *step size*, the Earth may have increased (or decreased) n_A by an amount dn_A, and Jupiter may have increased (or decreased) n_B by dn_B. Since n_A and n_B are really a measurement of the same density, and there are two processes (interactions with the two planets) affecting the differences, the orbit densities after the time step are given by

$$n_A\rightarrow n_A'=n_A+dn_A+Jdn_B,$$

$$n_B\rightarrow n_B'=n_B+dn_B+J^{-1}dn_A, \tag{45}$$

where J is the Jacobian for the transformation. Note that the step size introduced above is the step size after which trans-

fer of densities between planets occur. For the diffusion effects of the individual planets during this step size, we use much smaller time steps.

In order to transfer the orbit densities from one planet to another in a numerically reasonable way, all cells at each planet are matched to the correct cells on the other planet. Since there is not a one to one correspondence between the cells of different planets, we need to interpolate between cells. We use a linear interpolation, but have also checked that a simpler nearest neighbor interpolation gives similar (but more noisy) results.

The velocity spaces of all pairs of involved planets were tessellated in order to create the matrix of linear interpolation. This means that each cell was identified to constitute the corners of to up to six octahedrons. All transformed points were identified to belong to a single octahedron, and the location of the transformed point was given as a linear combination of the octahedron corners. This linear combination was then used as interpolation for the densities.

C. Numerical issues

In the preceding section, our scheme for taking care of the diffusion effects of more than one planet was outlined. We will here discuss the measures we have taken to make sure that our numerical implementation is stable and does not introduce numerical artifacts.

In order to further improve the stability of the interpolation between the planet cells, the orbit densities n are never interpolated directly. Instead, all interpolations are done between phase space densities F, and then converted to the n-space of the respective planets. The phase space density F is a slowly changing function, while n is not. This is so since among other things, the roughness of γ, Eq. (19), is included in n, but removed again when F is calculated.

At any time, the densities at the two planets must be consistent with each other so that a density at a particular point in one frame matches that of the point transformed to the other planet, as described by Eq. (43). Small interpolation errors can build up with time, though, and we need to take care of this potential problem. To force the densities at the two planets, n_A and n_B, to be consistent, they were regularly averaged, taking the Jacobians into account.

From an analytical point of view, this is not needed, but it turns out to be a good way of making the algorithm more numerically robust. We have verified that in the limit of very small step sizes, the unaveraged results approach the ones with averaging even in this region, but averaging allows us to get better accuracy and stability even with longer step sizes. In the steep region below $u=7$ km/s, averaging is needed though to keep the stability.

A related issue is that even though the Jacobian determinant of Eq. (44) is mathematically valid, linear interpolations do not ensure conservation of mass. This means that when repeatingly transferring density information between a pair of planets, one cannot be sure that the interpolation does not, in error, introduce or remove mass from the system. These artificial ''sources'' or ''sinks'' need to be removed. While it is not possible to do this on a cell by cell basis, we have investigated the total mass transferred to and from each planet and used this to renormalize the mass transferred to ensure mass conservation. In equilibrium, the correction is quite small; under one percent, but when a distribution is built up, the error can be larger than that.

The results are also well behaved with respect to step size as well as shape of the velocity space and frequency of averaging. This indicates that our numerical implementation, with the stability measures outlined above, is stable and that the possible errors are under control. The resulting figures of the preceding section show the results of a small step size: 16 thousand years.

D. Investigation of Jupiter-crossing orbits

It turns out that the density of Jupiter-crossing orbits is independent of the diffusion effects of the Earth as well as those of Venus. This is expected, since the mass of Jupiter is so much larger, and the scattering probability increases with the planet mass squared [see Eq. (23)].

To investigate this, we have numerically solved the Earth-Jupiter diffusion system in two ways: calculating the evolution with Jupiter alone, as well as solving the two-body diffusion problem with the methods described above. In either case, it takes only a couple of million years for Jupiter's Earth-crossing orbits to come into equilibrium with the unbound orbits. This means that for Jupiter-crossing orbits we can safely neglect the diffusion effects of the other planets and let Jupiter fill these orbits alone. It also turns out that the diffusion of Jupiter-crossing orbits is so much faster than solar depletion, and we can thus ignore solar depletion for these kind of orbits.

We can then already now see that the ultraconservative view in Gould and Alam [8] is too pessimistic and that at least as many bound WIMPs as in the conservative view remains in the solar system. We will next see what the fate is for bound orbits further inside the solar system.

E. Investigation of the Earth-Venus-Jupiter system

Inspired by the preceding section, we will from now on keep the density of Jupiter-crossing orbits constant and focus on the combined diffusion effects caused by Venus and the Earth. The locking of the Jupiter-crossing orbits is done in the same way as for the free orbits [see Eq. (34)], with the forced insertion of an identity matrix in the time evolution operator. As mentioned above, this is justified by the fact that diffusion of Jupiter-crossing orbits is so fast that we can view these orbits as constantly being filled from the halo. We also change the interpolations between the Earth and Venus so that Jupiter-crossing orbits are excluded (as they are filled by Jupiter).

Before going through the results, let us spend some time going through the diffusion processes in the low velocity region (as seen from the Earth). Figure 9 is a close view of the space of low-velocity orbits. If we ignore the filling effects of Jupiter, the Earth would have to diffuse WIMPs all the way from the unbound orbits, starting at the $u=12.3$ km/s sphere. They could eventually reach the Venus-crossing orbits to the left of the figure. Venus could then act

to diffuse the particles along *its* spheres of constant velocity. It is evident from the figure that the combined effect of the Earth and Venus could possibly populate all orbits outside the $u=2.5$ km/s line. By numerical simulation of the Earth-Venus system alone, it turns out that solar depletion is so strong that gravitational diffusion can only make a small contribution to the particle density below 12.3 km/s. This is no big surprise, since comparing the scattering times in Fig. 5 and the solar depletion times of Fig. 6, we see that solar depletion is indeed very strong.

If we instead use the knowledge about the density of Jupiter crossing orbits, the situation is very different. The Earth can scatter particles directly from the bound Jupiter crossing orbits, starting at $u\approx 8.8$ km/s, as opposed to 12.3 km/s for free orbits. Furthermore the time scale of scattering, as well as the angular path the WIMPs have to travel is much shorter, especially in the low velocity region. Hence, solar depletion will not be as effective when we include Jupiter, as the time scales for diffusion are more comparable to the solar depletion time scales.

In our full calculations, we will (as mentioned above) keep Jupiter-crossing orbits fixed and include Venus and the Earth in the diffusion process. The calculations start with a solar system empty of dark matter, five billion years ago. The step size (that is, how often the diffusion effects are added to the other planet) was usually some hundred thousand years. The first ten million years were typically calculated using smaller step sizes, such as 10 thousand years. The densities converge to their final values within a time of 500 million years. An example of the resulting phase space density at a sphere of constant velocity is given in Fig. 10. It is important to remember that the free distribution was averaged over a period of 100 million years. After such a time, the bound densities take on their final values within about 25%, which is an indication that the results might vary slightly during the galactic (half) year. In practice, this has little effect, since the typical time scales for equilibrium (see Sec. VII B) between capture and annihilation in the Earth are much longer than that and will average out these small variations over the galactic (half) year.

The resulting velocity distributions for the slowly moving particles are shown in Fig. 11. The ultraconservative and conservative curves represent the contributions from unbound and unbound plus Jupiter-crossing orbits, respectively. For these, we again see the cutoff velocities of 12.3 km/s and 8.8 km/s as explained in Sec. II B. The result of our full simulation, but ignoring solar depletion altogether, is also shown. It follows the Gaussian down to about 2.5 km/s where it drops to zero. This is in perfect agreement with the results of Gould [7], and we can see this agreement as a test that our numerical routines are performing as they should. Our full numerical routines without solar depletion is a numerical implementation of Gould's analytical arguments about diffusion in the solar system and our results should thus (as they do) agree in this case. We also show our raw numerical result, which is the outcome of our full simulation with solar depletion included. It is significantly lower than the Gaussian estimate in this low-velocity region, but not as low as the conservative (or ultraconservative) view. The general argument above that the time scales of solar depletion and diffusion are not too different and that some WIMPs should remain thus turns out to be valid. Hence, solar depletion kills some of the WIMPs at low velocities, but not as many as one could have feared. Also shown in the figure is our best estimate of the velocity distribution, which is the same as our raw numerical result, but modified at low ve-

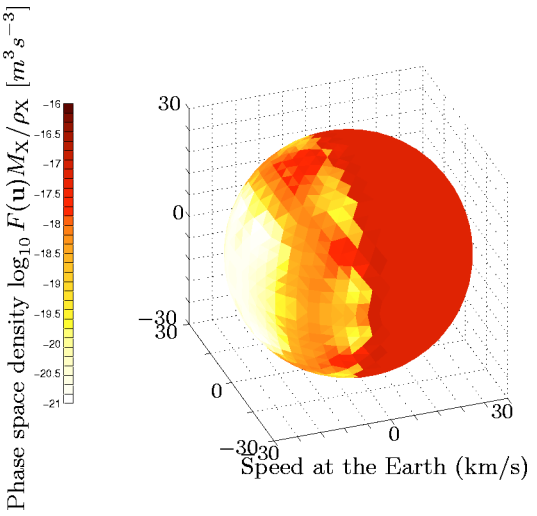

FIG. 10. (Color online). The final phase space distribution at the $u=30$ km/s sphere. In understanding this figure, it may help to take a look at the $u=30$ km/s line of Fig. 1, which corresponds to the central horizontal plane of this figure. The large red region to the right corresponds to unbound orbits. To the left (backwards 30 km/s) the phase space density is very low, as expected from the results of the solar depletion calculations. The leftmost part of the large red area corresponds to Jupiter crossing orbits, which are filled with the same density as the unbound orbits.

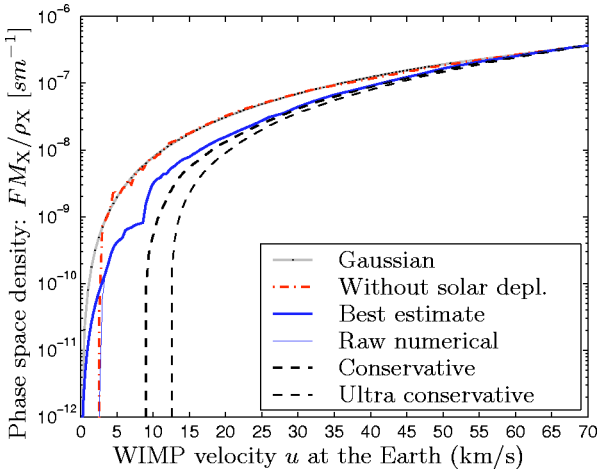

FIG. 11. (Color online). The radial velocity distribution of Earth crossing dark matter at the Earth. The curves labeled *conservative* and *ultraconservative* are the contributions from unbound, as well as unbound plus Jupiter crossing orbits, respectively. The dash-dotted curve displays the result of ignoring solar depletion. The blue solid line represents our best estimate, including the effect of the eccentricity of the Earth's orbit. The thin line is the raw result from the numerical routines.

locities (below 2.5 km/s) to include the effect of the eccentricity of the Earth's orbit, which will be explained now.

The diffusion effects included so far does not provide means of filling the extremely slow ($u<2.5$ km/s) orbits. Such processes arise when the eccentricity of the Earth's orbit is taken into account. This could be done in a way similar to ordinary diffusion, but since u would no longer be fixed even in the one-planet case, the block diagonal one-planet time evolution operator would be polluted with new, off-diagonal blocks, making the diffusion problem much more complicated. However, the eccentricity of the Earth's orbit will mean that the Earth diffuses slightly differently in different parts of its orbit. This will cause a mixing of spheres of different u and thus cause an effective diffusion in the $\hat{u}$ direction. The size of this effect can be estimated using Eq. (2.10) of Gould's paper [21]. Evaluation shows that for extremely slow particle orbits, the time scales can be as fast as one-tenth of those of the ordinary diffusion, while in most other cases they are far slower. It is therefore quite reasonable to ignore these effects in our diffusion treatment at higher velocities. For the $u<5$ km/s region the time scales of u diffusion is comparable to the time scales of solar depletion, which makes it reasonable to assume that the phase space density is a slowly changing function with respect to u, which means that the sharp cutoff at $u=2.5$ km/s is not physical. To estimate the phase space density at these very low velocities, the mean density in the $u\in[2.5,5]$ km/s region is calculated and used as a minimum density in the whole $u\in[0,5]$ km/s region. Another approach could have been to relocate the already existing mass to fill up the $u<5$ km/s region evenly. However, this would underestimate the density in the $u>2.5$ km/s region. Figure 12 compares the raw result of the full numerical simulations, with this new best estimate and the Gaussian. The conservative view is also shown for reference.

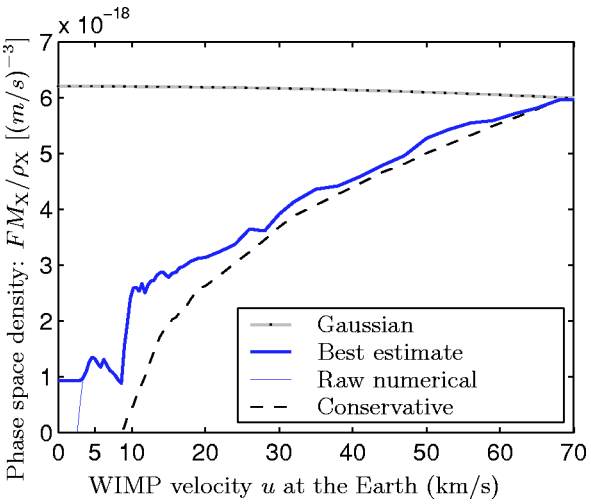

FIG. 12. (Color online). The phase space density $F(\mathbf{u})$ at low velocities. The upper curve is the Gaussian distribution. The thin solid curve is the outcome of our numerical simulations. The thick solid blue curve is our best estimate, where a population at low velocities (below 2.5 km/s) has been added due to the eccentricity of the Earth's orbit (see text). The dashed line, for comparison, shows the distribution in the conservative view where only unbound plus Jupiter-crossing orbits are included.

VII. CAPTURE AND ANNIHILATION RATES

In the preceding section, we have seen that our new estimate of the WIMP velocity distribution is, especially at low velocities, considerably lower than earlier estimates based on the Gaussian approximation [5]. We will here investigate how this new velocity distribution affects first the capture rates of WIMPs in the Earth and second the annihilation rates of WIMPs in the center of the Earth. In this section, we will keep the discussion general and in Sec. VIII we will investigate the effects for the neutralino as a WIMP dark matter candidate.

A. A new estimate of the capture rates . . .

Given the velocity distribution derived in the preceding section, we can now calculate the capture rate in the Earth with this velocity distribution. We will use the full expressions for the capture rate as derived by Gould in Ref. [4], but will also compare with the usual Gaussian approximation (as derived in Ref. [7]), as that is what most people use to calculate the capture rates.

The calculation of the capture rates for an arbitrary velocity distribution is given in Ref. [4], we will here only briefly outline how the calculation is done. We divide the Earth into shells, where the capture from element i in each shell (per unit shell volume) is given by [4] [Eq. (2.8)]

$$\frac{dC_i}{dV}=\int_0^{u_{max}}du\,\frac{\tilde{f}(u)}{u}w\Omega_{v,i}^{-}(w), \tag{46}$$

where $\tilde{f}(u)$ is the velocity distribution [normalized such that $\int_0^\infty\tilde{f}(u)=n_\chi$, where n_χ is the number density of WIMPs [34]]. The expression $\Omega_{v,i}^{-}(w)$ is related to the probability that we scatter to orbits below the escape velocity. w is the velocity at the given shell and it is related to the velocity at infinity u and the escape velocity v by $w=\sqrt{u^2+v^2}$. The upper limit of integration, u_{max}, is set to the kinematical limit for capture to be possible. We refer the interested reader to Appendix A of Ref. [4] for details. Included in $\Omega_{v,i}^{-}(w)$ is a dependence on the scattering cross section off element i, for which we use the expression in Ref. [12] [Eqs. (9–25)]

$$\sigma_i=\sigma_p A_i^2\frac{(m_\chi m_i)^2}{(m_\chi+m_i)^2}\frac{(m_\chi+m_p)^2}{(m_\chi m_p)^2}, \tag{47}$$

where A_i is the atomic number of the element, m_p is the proton mass, and σ_p is the scattering cross section on protons.

We now have what we need to calculate the capture rate. In Eq. (46) we integrate over the velocity for our chosen velocity distribution. We then integrate this equation over the radius of the Earth and sum over all the different elements in the Earth,

TABLE I. The composition of the Earth's core and mantle. The core mass fractions are from Table 4 in Ref. [22] and the mantle mass fractions are from Table 2 in Ref. [22].

Element	Atomic number	Mass fraction Core	Mass fraction Mantle
Oxygen, O	16	0.0	0.440
Silicon, Si	28	0.06	0.210
Magnesium, Mg	24	0.0	0.228
Iron, Fe	56	0.855	0.0626
Calcium, Ca	40	0.0	0.0253
Phosphor, P	30	0.002	0.00009
Sodium, Na	23	0.0	0.0027
Sulfur, S	32	0.019	0.00025
Nickel, Ni	59	0.052	0.00196
Aluminum, Al	27	0.0	0.0235
Chromium, Cr	52	0.009	0.0026

$$C = \int_0^{R_\oplus} dr \sum_i \frac{dC_i}{dV} 4\pi r^2. \tag{48}$$

The capture rates depend on the mass and distribution of the elements in the Earth. The most important elements are iron, silicon, magnesium, and oxygen, of which iron is by far most important for WIMP masses over 100 GeV. We use the Earth density profile as given in Ref. [20] and for the element distribution within the Earth we use the values given in Table 2 for the mantle and Table 4 for the core from Ref. [22]. These values are listed in Table I.

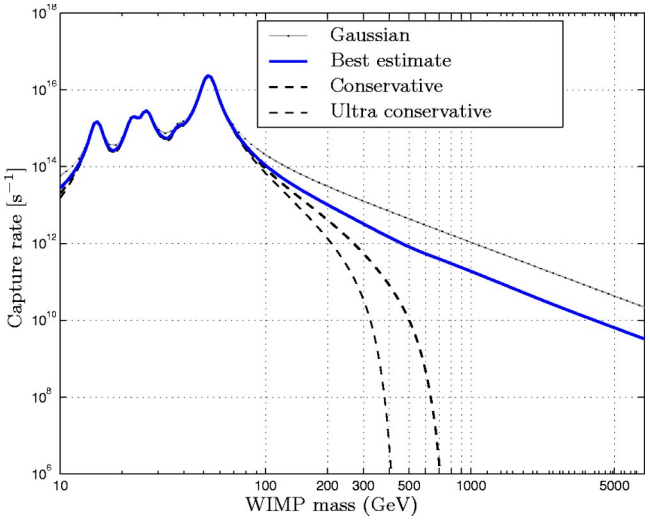

FIG. 13. The capture rate of dark matter. This figure shows the rate at which dark matter particles are captured to the interior of the Earth, for a scattering cross section of $\sigma = 10^{-42}$ cm^2. The Gaussian–no solar depletion model gives the highest capture. The curves labeled *ultraconservative* and *conservative* are the contributions from unbound, as well as unbound plus Jupiter-crossing orbits, respectively. For masses above 150 GeV, our new capture estimate is considerably lower than that of the Gaussian model. The peaks at low WIMP mass correspond to the masses of the included elements. A dark matter halo density of $\rho_X = 0.3$ GeV/cm^3 is assumed.

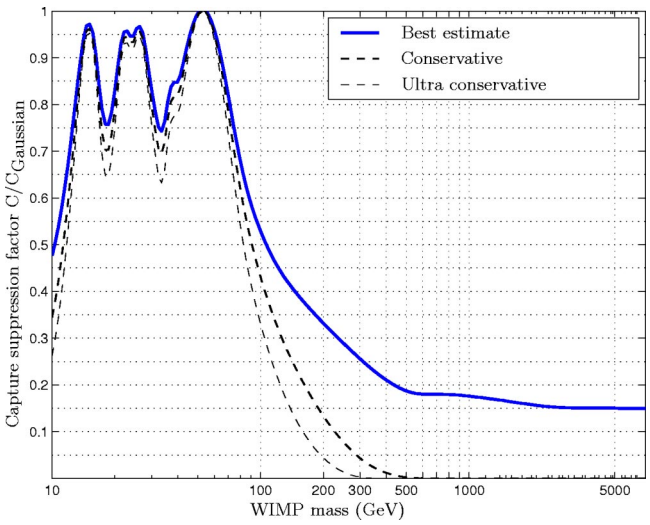

FIG. 14. The ratio between the capture in various models and that of a Gaussian distribution in free space. The figure displays the quotient of the weak WIMP capture rates in the Earth in various models, and the capture given in the case of the commonly used Gaussian distribution.

Figure 13 shows the calculated capture rates, to be compared with that of a Gaussian distribution, with the Earth in free space. The Gaussian distribution is the one of Eq. (3) in Sec. II A. The scattering cross section between the nucleons and the WIMPs determines the normalization only, and was taken to be 10^{-42} cm^2 in Fig. 13. We also show the resulting capture rates in the conservative and ultraconservative view, where the cutoffs at about 710 GeV and 410 GeV are clearly seen. These cutoff masses are higher than those given by Gould and Alam [8] as we have used the full integration over the Earth and not the average properties as in Ref. [8] (see Sec. II B for a discussion of these cutoff masses).

It is of course interesting to compare the calculated capture rate with that given by the commonly used Gaussian distribution. This is done in Fig. 14, where we divide by the capture rate in the Gaussian approximation. We clearly see that below 100 GeV, the different calculations agree to within about a factor of two. At higher masses the suppression is almost an order of magnitude, but not as bad as the feared conservative or ultraconservative views.

B. . . . and the annihilation rates

We have seen that our new estimate of the capture rate in the Earth is, especially at higher masses, considerably lower than the usual estimate based on the Gaussian approximation [7]. Since the neutrino-induced muon rates do not directly depend on the capture rate, but instead on the annihilation rate, we will here investigate how the annihilation rates are affected.

The evolution equation for the number of WIMPs, N, in the Earth is given by

$$\frac{dN}{dt} = C - C_A N^2 - C_E N, \tag{49}$$

where the first term is the WIMP capture, the second term is twice the annihilation rate $\Gamma_A = \frac{1}{2} C_A N^2$, and the last term is WIMP evaporation. The evaporation term can be neglected for WIMPs heavier than about 5–10 GeV [4] and since we are not interested in these low-mass WIMPs we can safely drop the last term in Eq. (49). If we solve Eq. (49) for the annihilation rate Γ_A we get

$$\Gamma_A = \frac{1}{2} C \tanh^2 \frac{t}{\tau}, \quad \tau = \frac{1}{\sqrt{C C_A}}, \tag{50}$$

where τ is the time scale for capture and annihilation equilibrium to occur. In the Sun, equilibrium will for many WIMP models have occurred and the annihilation rate is at ''full strength,'' $\Gamma_A \simeq \frac{1}{2} C$. In this case the annihilation rate is directly proportional to the capture rate. However, in the Earth, equilibrium has often not occurred, and we will have the more complex relation between the capture and annihilation rate, Eq. (50). In the next section, we will show this for an explicit example, the neutralino in the minimal supersymmetric standard model (MSSM). Before looking at specific MSSM models, let us analyze Eq. (50) to see the general trends. Let us denote the capture and annihilation rates in the usual Gaussian approximation by C^G and Γ_A^G, respectively, whereas our new estimates are denoted C and Γ_A. Using the fact that the constant C_A is the same in both scenarios, we can then write

$$\frac{\Gamma_A}{\Gamma_A^G} = \frac{C}{C^G} \frac{\tanh^2\left(\sqrt{\frac{C}{C^G}} \frac{t_\odot}{\tau} \right)}{\tanh^2\left(\frac{t_\odot}{\tau} \right)} \simeq \begin{cases} \frac{C}{C^G}, & t_\odot \gg \tau \\ \left(\frac{C}{C^G} \right)^2, & t_\odot \ll \tau. \end{cases} \tag{51}$$

Hence, if equilibrium has occurred, the annihilation rate (and thus the neutrino-induced muon fluxes) are suppressed with the same factor as the capture rates, but if equilibrium has not occurred, the annihilation rate is suppressed with the square of the capture rate suppression factor, i.e., the suppression is amplified.

VIII. APPLICATION TO THE SUPERSYMMETRIC NEUTRALINO

So far, we have discussed the effects of our new estimate of the velocity distribution in general terms. We have seen that our estimate of the velocity distribution is significantly different from previous estimates at low velocities. We have also seen that the capture rates, especially at higher WIMP masses, are significantly reduced with a factor C/C^G. Hence, the annihilation rates (and the expected neutrino-induced muon fluxes) are reduced by a factor that lies between $(C/C^G)^2$ and C/C^G. We now want to investigate this suppression factor further and analyze the effects on the neutrino-induced muon fluxes. For this we need an explicit WIMP candidate. We will here assume that the WIMP is the lightest neutralino, which arises as a natural dark matter candidate in supersymmetric extensions of the standard model. In the following section, we will briefly go through the supersymmetric model we work in and will then continue to investigate the effects of our new velocity distribution on the annihilation rates and the neutrino-induced muon fluxes.

A. The neutralino as a dark matter candidate

We will assume that the WIMP is the lightest neutralino in the MSSM, i.e., the lightest neutralino, $\tilde{\chi}_1^0$, is defined as the lightest mass eigenstate obtained from the superposition of four spin-1/2 fields, the B-ino and W-ino gauge fields, $\tilde{B}$ and $\tilde{W}^3$, and two neutral CP-even Higgsinos, $\tilde{H}_1^0$ and $\tilde{H}_2^0$. For a recent review of the MSSM and the neutralino as a dark matter candidate, see Ref. [23]. The parameters of our phenomenologically inspired MSSM model are the Higgsino mass parameter μ, the gaugino mass parameter M_2, the ratio of the Higgs vacuum expectation values $\tan\beta$, the sfermion mass scale $M_{\tilde{q}}$, the mass of the CP-odd Higgs boson m_A, and the trilinear couplings for the third generation squarks A_t and A_b. We have made extensive scans of these parameters and have currently about a couple of hundred thousand models in our model database.

For our actual calculations we use the DarkSUSY package [24]. We only select those models that do not violate present accelerator bounds. The neutralino naturally has a relic density in the right range, and we will further restrict this range by selecting only models with a relic density in the range $0.05 \leqslant \Omega_\chi h^2 < 0.2$. This range is a bit larger than the current best estimates [1], but to be conservative we choose to work with this larger range. When calculating the relic density, we have included coannihilations between neutralinos and charginos (coannihilations also with sfermions in the MSSM is the subject of a future publication).

B. Neutralino capture and annihilation

We will investigate here how the annihilation rates are affected for specific MSSM models. For our large set of MSSM models, the typical equilibrium time scales $\tau \sim 10^{17}$–10^{23} s, i.e., longer or much longer than the age of the solar system, $t_\odot \simeq 4.5 \times 10^9$ years. Hence, equilibrium between capture and annihilation has often not occurred in the Earth. As equilibrium has not occurred in the Earth, we can use Eq. (50) to see how the decrease in C will affect Γ_A.

In Fig. 15 we show, for a set of MSSM models, how the annihilation rates are decreased. We also show the limiting cases for $t_\odot \gg \tau$ and $t_\odot \ll \tau$. We can clearly see that for most models, as equilibrium has not occurred, we are close to the $(C/C^G)^2$ suppression of the annihilation rates.

C. Neutrino-induced muon fluxes from the Earth

So, given our calculated suppression of the annihilation rates, the neutrino-induced muon fluxes will also be suppressed by the same amount. We now ask ourselves if this suppression is too big to make the neutrino-induced muon fluxes too low to be observable in the MSSM. In Fig. 16 we

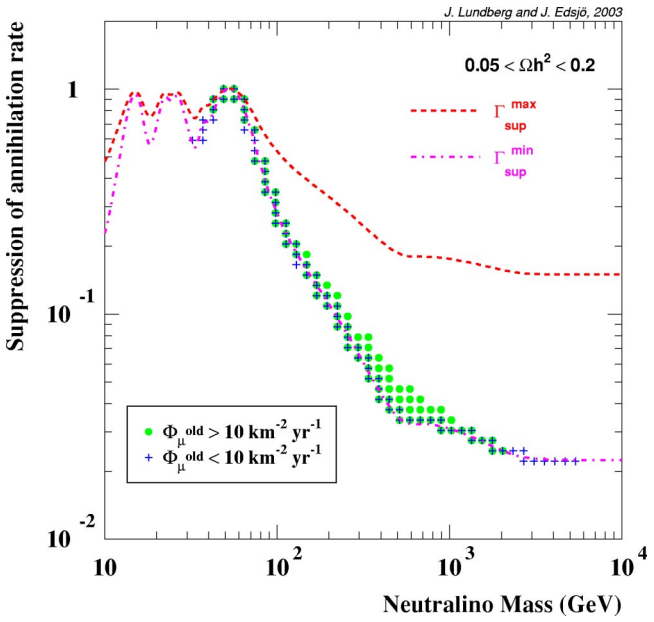

FIG. 15. Γ_A/Γ_A^G versus the neutralino mass m_χ. The limiting cases for $t_\odot \gg \tau$ and $t_\odot \ll \tau$ are indicated in the figure. Most models have annihilation rate suppressions close to the lower curve since equilibrium has most often not occurred in the Earth.

show in the left panel the neutrino-induced muon fluxes with the old Gaussian approximation. In the right panel, we show the neutrino-induced fluxes with our new estimate of the WIMP velocity distribution. We also indicate current limits from neutrino telescopes (Baksan [26], Macro [27], Amanda [28], and Super-Kamiokande [29]) and anticipated sensitivities for future neutrino telescopes like IceCube [30]. Note that the IceCube limit shown here is a probably too optimistic, but we show it as limiting case beyond which a 1 km^3 neutrino telescope will not reach. For comparison, we also indicate the current direct detection limit by the Edelweiss experiment [25]. Models that are excluded by Edelweiss are indicated by green circles, whereas models that are not excluded are indicated with blue crosses.

Comparing the left and the right figures, we clearly see that there is a significant suppression of the rates above about 100 GeV, and above about 2000 GeV, the fluxes are too low to be observable even with future detectors. In the range between 100 GeV and 2000 GeV, where future neutrino telescopes still have a chance to detect a signal from the Earth, the prospects for doing so are clearly diminished with our new estimate of the fluxes, especially if one considers that all of the observable models in that range are already excluded by direct detection experiments. Note, however, that the comparison between direct detection and neutrino telescopes that we have done here is for a Maxwell-Boltzmann velocity distribution. As direct detection experiments are primarily sensitive to the high velocity tail of the distribution, whereas neutrino telescopes are sensitive to the low velocity tail, the correlation between the two signals need not be as large as indicated in Fig. 16 for a more realistic distribution. Below 100 GeV, the neutrino signal from the Earth is not reduced much with our new velocity distribution. In this range, neutrino telescopes are also in general more sensitive than direct detection experiments.

IX. CONCLUSIONS

We have made a new estimate of the velocity distribution of WIMPs at the Earth due to diffusion in the solar system.

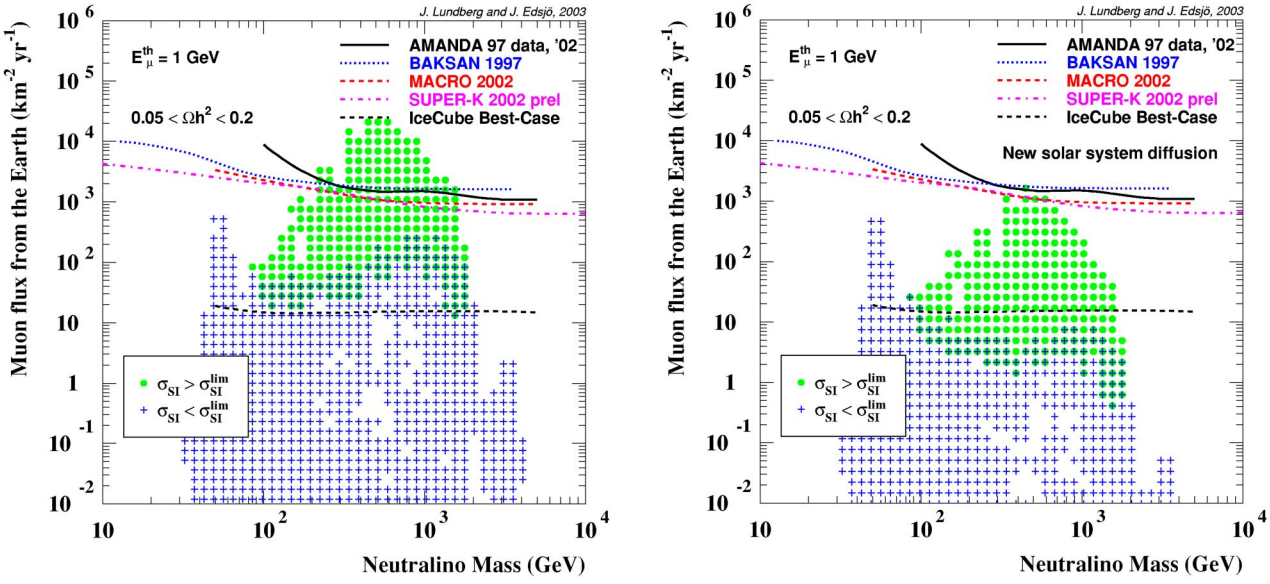

FIG. 16. (Color online). In the left panel we show the neutrino-induced muon fluxes in the standard Gaussian approximation, whereas in the right panel we show the fluxes based on our new estimate of the WIMP diffusion in the solar system. We also show the current limits of a few neutrino telescopes and an optimistic estimate for the future IceCube sensitivity. The current direct detection limit by the Edelweiss experiment [25] is also shown. Models that are excluded by Edelweiss are indicated by green circles, whereas models that are not excluded are indicated with blue crosses.

We have included gravitational diffusion due to the Earth, Venus, and Jupiter and depletion due to solar capture. Compared to the standard approximation (i.e., that the solar diffusion can be approximated by the Earth being in free space and seeing the unperturbed Gaussian halo velocity distribution), our estimate is significantly lower at low velocities (below about 70 km/s). The main reason for this is that solar capture diminishes the WIMP population at these low velocities. If it were not for solar capture, our results would confirm the results of Gould [7], i.e., that the velocity distribution as seen at the Earth is close to the one in free space. The diffusion effects of Jupiter, Earth, and Venus would make the distribution look Gaussian, apart from a hole in the distribution below 2.5 km/s. This hole would, however, be filled due to the eccentricity of the Earth's orbit. However, solar capture suppresses the velocity distribution by about an order of magnitude at low velocities and this suppression propagates into a suppression of the same order of magnitude in the capture rate.

Since the annihilation rates depend on the capture rates, the annihilation rates are also suppressed. The amount of suppression, however, depends on whether capture and annihilation are in equilibrium or not. If they are in equilibrium the annihilation rate suppression is the same as the capture rate suppression, but if we are not in equilibrium, the annihilation rate suppression is equal to the capture rate suppression squared.

For one of the prime WIMP dark matter candidates, the neutralino in the MSSM, it turns out that these are typically not in equilibrium, and thus the annihilation rate suppression is equal to the capture rate suppression squared. The net result is that the annihilation rates will start being suppressed above about 100 GeV, and reaches a maximal suppression of about 10^{-2} at around 1 TeV. Above about 2 TeV, the expected fluxes are so low that future neutrino telescopes will not have enough sensitivity to see these.

Finally, a word of caution should be applied to the interpretation of these new results. Even if we have done what we can to make sure that our new estimate is correct, there are still approximations done and numerical uncertainties that need to be considered. For example, in principle one would like to do a full numerical simulation of the full diffusion process with an arbitrary halo distribution as input. That is not numerically feasible to do so; instead we have relied on numerical simulations for the solar capture and on analytical calculations and arguments for the diffusion process. These analytical calculations are approximations with the aim to describe the diffusion processes correctly on average. We think that these approximations are reasonable, but one should keep in mind that there are uncertainties involved in these approximations. At higher masses, above about 1 TeV, we are very sensitive to the very details of the velocity distribution at very low velocities (a few km/s). We have assumed that the eccentricity of the Earth's orbit fills the hole below 2.5 km/s. If this would not be the case, the suppression for high masses would be even larger than depicted here.

TABLE II. The asteroids integrated by Farinella *et al.* The numbers given are the times at which the asteroid collided with the Sun, or was ejected, in thousands of years. The asterisks mark asteroids we have not calculated. The following asteroids survived the full two million year period, according to Farinella *et al.* and our calculation (and are not included in the table): 1972 RB, 1981 QB, 1981 QN1, 1982 TA, 1984 KB**, 1990 OA, 1990 SM, 1991 EE, 1991 VC, 1992 EU, 1992 RD, 1992 SY, 1992 SZ, 1998 CC1, 1998 PA, Beltrovata, Dionysus, Dorchester, Grieve, Hiltner, Krok, Oljato, Poseidon, Taurinensis, Verbano, Verenia, Wisdom, Zeus.

	MERCURY pack		Farinella *et al.*	
1971 SC		**	Sun	1400
1983 LC	Sun	42	Sun	810
1988 NE	Sun	1062	Sun	950
1988 VP_4		**	Sun	1470
1989 DA	Sun	369		
1990 HA	Sun	1985	Eject	450
1990 TG_1	Eject	362	Eject	420
1990 TR	Eject	1449		
1991 AQ	Sun	456		
1991 BA			Sun	120
1991 GO			Sun	600
1991 SZ			Sun	1860
1991 TB_2	Sun	625	Sun	30
1991 VP_5		**	Sun	570
1992 SY	Sun	1509		
6344 P-L	Eject	362		
Adonis	Sun	1214	Sun	900
Cuno	Sun	1274	Eject	640
Encke			Sun	90
Hephaistos	Sun	143	Sun	110
Mithra	Sun	205	Sun	180
Ojato	Sun	328	Sun	360
Toutatis	Eject	79	Eject	640

ACKNOWLEDGMENT

We thank A. Gould for comments. J.E. thanks the Swedish Research Council for support.

APPENDIX: COMPARISON WITH FARINELLA'S CALCULATION OF NEAR EARTH ASTEROIDS

This appendix considers the 47 asteroids (mostly near Earth asteroids, NEAs), whose fates were investigated by Farinella *et al.* [9]. As a test of the MERCURY integration package [14], we have repeated the calculations of Farinella *et al.* using both the Bulirsch-Stoer algorithm [16] and fifteenth-order Radao algorithm [15].

The actual fates of specific asteroids is of course dependent of the method used, and the accuracy parameters of the calculation. Even with very high accuracy, convergence cannot be expected since numerical errors propagate exponentially in chaotic systems. The initial conditions of our calculations are those of the online asteroid database at U.S. Naval Observatory, epoch 11-22-2002. In addition to the time

passed, some asteroids have been observed many times since 1994. However, one can still hope to imitate the general behavior by looking at a large set of initial values, regardless of what they represent; asteroids or WIMPs.

The results for the Bulirsch-Stoer method are presented in Table II. Of the 47 objects, four were ejected from the solar system and twelve were captured by the Sun in our calculations, whereas four were ejected and 14 were captured by the Sun in the Farinella *et al.* calculations. We cannot expect to get exactly the same results on an individual basis, but are satisfied to see that we get roughly the same behavior as Farinella *et al.*

[1] C.L. Bennett *et al.*, Astrophys. J., Suppl. Ser. **148**, 1 (2003).

[2] K. Freese, Phys. Lett. **167B**, 295 (1986); L. Krauss, M. Srednicki, and F. Wilczek, Phys. Rev. D **33**, 2079 (1986); T. Gaisser, G. Steigman, and S. Tilav, *ibid.* **34**, 2206 (1986).

[3] W.H. Press and D.N. Spergel, Astrophys. J. **296**, 679 (1985).

[4] A. Gould, Astrophys. J. **321**, 571 (1987).

[5] A. Gould, Astrophys. J. **328**, 919 (1988).

[6] E. Öpik, *Interplanetary Encounters: Close-Range Gravitational Interaction* (Elsevier Scientific, Amsterdam, 1976).

[7] A. Gould, Astrophys. J. **368**, 610 (1991).

[8] A. Gould and S.M.K. Alam, Astrophys. J. **549**, 72 (2001).

[9] P. Farinella, C. Froeschlé, C. Froeschlé, R. Gonczi, G. Hahn, A. Morbidelli, and G.B. Velsecchi, Nature (London) **371**, 314 (1994).

[10] B. Gladman *et al.*, Science **277**, 197 (1997).

[11] F. Migliorini *et al.*, Science **281**, 2022 (1998).

[12] G. Jungman, M. Kamionkowski, and K. Griest, Phys. Rep. **267**, 195 (1996).

[13] F. Scheck, *Mechanics: From Newton's Laws to Deterministic Chaos*, 3rd ed. (Springer-Verlag, Berlin, 1999).

[14] J.E. Chambers, Mon. Not. R. Astron. Soc. **304**, 793 (1998).

[15] E. Everhart, in Proceedings of the International Astronomical Union, Rome, Italy, 1984, *Dynamics of Comets: Their Origin and Evolution*, edited by A. Carusi and G.B. Valsecchi (Reidel, Dordrecht, 1985).

[16] J. Stoer and R. Bulirsch, in 1992, *Numerical Recipes in Fortran*, edited by W.H. Press *et al.* (Cambridge University Press, Cambridge, 1992).

[17] J. Wisdom and M. Holman, Astrophys. J. **102**, 1528 (1991); J. Wisdom, M. Holman, J. Touma, in *Intergration Algorithms and Classical Mechanics*, edited by J.E. Marsden, G.W. Patrick, and W.F. Shadwich, Fields Institute Communications, Vol. 10 (American Mathematical Society, Providence, 1996), p. 10.

[18] S.I. Ipatov and J.C. Mather, "*Migration of the Jupiter-family comets and resonant asteroids to near-Earth space*," astro-ph/0303219.

[19] T. Guillot, Planet. Space Sci. **47**, 1183 (1999).

[20] *The Earth: Its Properties, Composition, and Structure*, Britannica CD (Encyclopædia Britannica, Chicago, 1999), Version 99.

[21] A. Gould, Astrophys. J. **388**, 338 (1992).

[22] W.F. Mcdonough, *Treatise on Geochemistry* (Elsevier, Oxford, 2003), Vol. 2. [The values for the Earth composition are very close to those in *The Encyclopedia of Geochemistry*, edited by C.P. Marshall and R.W. Fairbridge (Kluwer Acadmic, Dordrecht, 1998)].

[23] L. Bergström, Rep. Prog. Phys. **63**, 793 (2000).

[24] P. Gondolo, J. Edsjö, P. Ullio, L. Bergström, M. Schelke, and E.A. Baltz, "DarkSUSY—*A numerical package for supersymmetric dark matter calculations*," astro-ph/0211238.

[25] A. Benoit *et al.*, Phys. Lett. B **545**, 43 (2002).

[26] M. Boliev *et al.*, in *Proceedings of Dark Matter in Astro and Particle Physics, 1997*, edited by H. V. Klapdor-Kleingrothaus and Y. Ramachers (World Scientific, Singapore, 1997), p. 711. See also O. Suvorova, hep-ph/9911415.

[27] M. Ambrosio *et al.*, Phys. Rev. D **60**, 082002 (1999).

[28] J. Ahrens *et al.*, Phys. Rev. D **66**, 032006 (2002).

[29] A. Habig *et al.*, in Proceedings of the XVII International Cosmic Ray Conference (ICRC), Hamburg, Germany, 2001, p. 1558 (hep-ex/0106024); S. Desai, talk at Identificaiton of Dark Matter, 2002 (idm2002), York, England.

[30] J. Edsjö, internal Amanda/IceCube report, 2000.

[31] Gould and Alam [8] used parameters valid for general orbits, whereas we used parameters relevant for determining the cutoff accurately.

[32] It is unclear if Venus has a liquid iron core or not. Our results are not sensitive to this, and we choose a model with only a solid iron core.

[33] Note that if du is not small, the volume of the cell is not $d\Omega u^2 du$, but $\Omega u^2 du[1+du^2/(12u^2)]$. When numerical values are called for, we use the latter expression for accurate results.

[34] We introduce the velocity distribution $\tilde{f}(u)$ here to be as close as possible to Gould's expressions. This distribution is related to $F(u)$ in Sec. II A through $\tilde{f}(u)=4\pi u^2 F_u(u)$.